

## Article

# Study of Photocatalytic Oxidation of Micropollutants in Water and Intensification Case Study

Lucija Radetić <sup>1</sup> , Jan Marčec <sup>1</sup>, Ivan Brnardić <sup>2</sup>, Tihana Čižmar <sup>3</sup> and Ivana Grčić <sup>1,\*</sup> <sup>1</sup> Faculty of Geotechnical Engineering, University of Zagreb, Hallerova Aleja 7, HR-42000 Varaždin, Croatia<sup>2</sup> Faculty of Metallurgy, University of Zagreb, Aleja Narodnih Heroja 3, HR-44000 Sisak, Croatia<sup>3</sup> Ruđer Bošković Institute, Bijenička 54, HR-10000 Zagreb, Croatia

\* Correspondence: igrcic@gfv.hr or ivana.grcic@gfv.unizg.hr

**Abstract:** During the last decades, heterogenous photocatalysis has shown as the most promising advanced oxidation process for the removal of micropollutants due to degradation rate, sustainability, non-toxicity, and low-cost. Synergistic interaction of light irradiation, photocatalysts, and highly reactive species are used to break down pollutants toward inert products. Even though titanium dioxide (TiO<sub>2</sub>) is the most researched photocatalyst, to overcome shortcomings, various modifications have been made to intensify photocatalytic activity in visible spectra range among which is modification with multiwalled carbon nanotubes (MWCNTs). Therefore, photocatalytic oxidation and its intensification by photocatalyst's modification was studied on the example of four micropollutants (diclofenac, DF; imidacloprid, IMI; 1-H benzotriazole, BT; methylene blue, MB) degradation. Compound parabolic collector (CPC) reactor was used as, nowadays, it has been considered the state-of-the-art system due to its usage of both direct and diffuse solar radiation and quantum efficiency. A commercially available TiO<sub>2</sub> P25 and nanocomposite of TiO<sub>2</sub> and MWCNT were immobilized on a glass fiber mesh by sol-gel method. Full-spectra solar lamps with appropriate UVB and UVA irradiation levels were used in all experiments. Photocatalytic degradation of DF, IMI, BT, and MB by immobilized TiO<sub>2</sub> and TiO<sub>2</sub>/CNT photocatalysts was achieved. Mathematical modelling which included mass transfer and photon absorption was applied and intrinsic reaction rate constants were estimated:  $k_{DF} = 3.56 \times 10^{-10} \text{s}^{-1} \text{W}^{-0.5} \text{m}^{1.5}$ ,  $k_{IMI} = 8.90 \times 10^{-11} \text{s}^{-1} \text{W}^{-0.5} \text{m}^{1.5}$ ,  $k_{BT} = 1.20 \times 10^{-9} \text{s}^{-1} \text{W}^{-0.5} \text{m}^{1.5}$ ,  $k_{MB} = 1.62 \times 10^{-10} \text{s}^{-1} \text{W}^{-0.5} \text{m}^{1.5}$ . Intensification of photocatalysis by TiO<sub>2</sub>/CNT was observed for DF, IMI, and MB, while that was not the case for BT. The developed model can be effectively applied for different irradiation conditions which makes it extremely versatile and adaptable when predicting the degradation extents throughout the year using sunlight as the energy source at any location.

**Keywords:** micropollutants; TiO<sub>2</sub> films; TiO<sub>2</sub>/CNT nanocomposites; photocatalysis kinetics

**Citation:** Radetić, L.; Marčec, J.; Brnardić, I.; Čižmar, T.; Grčić, I. Study of Photocatalytic Oxidation of Micropollutants in Water and Intensification Case Study. *Catalysts* **2022**, *12*, 1463. <https://doi.org/10.3390/catal12111463>

Academic Editors: Rafael Borja, Gassan Hodaifa and Mha Albqmi

Received: 9 October 2022

Accepted: 14 November 2022

Published: 18 November 2022

**Publisher's Note:** MDPI stays neutral with regard to jurisdictional claims in published maps and institutional affiliations.



**Copyright:** © 2022 by the authors. Licensee MDPI, Basel, Switzerland. This article is an open access article distributed under the terms and conditions of the Creative Commons Attribution (CC BY) license (<https://creativecommons.org/licenses/by/4.0/>).

## 1. Introduction

Advancement of technology has contributed to humankind progresses, but at the same time, there is the consequence of dealing with the environmental pollution and energy crisis [1]. Furthermore, advances in analytical methods have enabled detection of previously unknown compounds as well as their occurrence in the environment. Consequently, conventional wastewater treatment plants (WWTPs) were recognized as a key source of micropollutants since they are not designed for elimination of trace concentrations [2–4]. Pharmaceuticals, pesticides, personal care products, steroid hormones and other organic compounds were detected in effluents after WWTPs as well as in the environment at concentration levels ranging between  $\text{ng}\cdot\text{L}^{-1}$  and  $\mu\text{g}\cdot\text{L}^{-1}$  [5]. Even though removal of micropollutants is not mandatory in the European Union, up to now, three watch lists were established in order to monitor, collect data, and assess the potential risk for the environment and humans [4].

In this work, four micropollutants were chosen, each representing a field of application. Diclofenac (DF) is a substance commonly used as a pharmaceutical due to its anti-inflammatory properties. Therefore, it is one of the 12 most consumed drugs in the world. It has been detected in wastewaters, surface, and underground waters [6–8] since 65% of its initial oral dosage is eliminated as unmodified or metabolites through urine or feces [9], with removal rate of DF in the range of 21–40% after WWTPs [7,8]. At low concentrations, effects like cytotoxicity to kidney, liver and gill cells along with renal lesions were reported in literature [2]. Imidacloprid (IMI) is a widely used pesticide and belongs to neonicotinoid group of pesticides. It is used as an insecticide and has seed protection properties [10]. It is harmful for the pollinators [10], while its degradation products poses a risk to vertebrates, mammals, and humans [11]. Due to its wide application, IMI has been detected in surface waters and soil sediments, behaving as a hormone disruptor causing obesity and reproductive imbalance in organisms [12]. The importance of DF and IMI occurrence in surface waters was recognized as they were listed in first (both) and second (IMI) watch lists [4]. Another compound that is widely used in industrial activities and everyday life is 1H-benzotriazole (BT) [13]. Its application varies from corrosive inhibition in deicing fluids to application in bleaching, antifogging, and antifungal agents [14–17]. Moreover, it is formed during the synthesis of dyes, drugs, and fungicides as intermediates [13]. About 9000 tons of BT are produced annually [18,19] with airports being the hot spots of the BT releasement in the environment [13,20]. It has been estimated that approximately 30% of the total BT input into wastewaters are due to discharge from dishwashing machines [20]. Considering their wide application and yet low removal rate in WWTPs [21], and at same time chemical stability and high-water solubility, BT's residuals were detected mainly in aquatic environments in concentrations from nano to micro gram per liter [22–24]. Even though reported acute toxicity is generally low, considerable residuals levels were found in various organisms revealing a potential risk. In a lettuce leaf and strawberry, 153 and 44  $\text{ng}\cdot\text{g}^{-1}$  BT were found [25,26]. In the Yangtze and Pearl rivers in China, the maximum concentration of BT in wild fish was 2950  $\text{ng}\cdot\text{L}^{-1}$  [27–29]. In human urine, a maximum 24.5  $\mu\text{g}\cdot\text{L}^{-1}$  of BT and its derivatives were determined [30]. Endocrine disrupting effects, hepatotoxicity, and neurotoxicity are some of the effects related with the sublethal dosages and bioaccumulation effects [13,14]. Even though, research about impacts on human health are scarce [20],  $\text{LC}_{50}$  concentration of BT causing 50% mortality in the *Ceriodaphnia dubia* (48 h) and *Pimephales promelas* (96 h) were 86–120 and 38–75  $\text{mg}\cdot\text{L}^{-1}$ , respectively [31]. Methylene blue (MB) is often used as a reference measurement to test photocatalytic activity of the prepared photocatalyst [32–40]. It's a very soluble synthetic dye with wide application in industry, such as paper, textile, chemical industry, as well in medical procedures [41]. It was reported that around 15% to 20% of the overall world production of dyes are lost during the dyeing process [42,43], which is significant since usually less than 1 ppm is sufficient to produce coloration of water and consequently reduce photosynthetic activity in the aquatic flora [43]. Since biodegradation process is slow, its removal is of interest [44].

Low-rate removal of contaminants from effluents and their occurrence in surface and underground waters have been directing efforts towards research of environmentally friendly techniques. Therefore, advanced oxidation processes (AOPs) are of considerable interest due to their feasible application in WWTPs [3,4,45]. Out of AOPs, heterogenic photocatalysis is one of the most promising. The basic principle can be described with the band gap model, according to which electrons from valence band are transferred into conduction band when photons ( $h\nu$ ) induce the photocatalyst's surface with energy that is equal or higher than the photocatalyst's band gap energy ( $E_g$ ), forming an electron–hole pair ( $h^+/e^-$ ) [46] crucial for the initiation of redox processes. Prior to photocatalytic redox processes that occur on the photocatalyst surface, diffusion of pollutants and reactants takes place, followed by their adsorption on active sites. Simultaneously, desorption of the oxidized/reduced byproducts occurs and diffuses in the solution participating in new redox processes [6]. In those processes, powerful oxidizing species, hydroxyl radicals, are

formed, which non-selectively mineralize pollutants to thermodynamically stable oxidation products such as CO<sub>2</sub>, H<sub>2</sub>O, and inorganic ions [3,47].

Semiconductors, especially, ZnO and TiO<sub>2</sub> have been recognized as the most effective photocatalysts [1]. The most researched one has been TiO<sub>2</sub> due to its cost, non-toxicity, and photochemical stability, with high photoactivity and mineralization efficiency. However, the drawback is its photocatalytic activity only in UV range ( $\lambda \leq 390$  nm), and relatively high rate of electron–hole pairs recombination which reduces available charges for the redox reactions [3,48]. To overcome the shortcomings, various modifications have been made in order to intensify photocatalytic activity in the visible spectra range [1] which has huge potential from an environmental and economic point of view [49]. The aim of modifications is to form a localized state just above the conduction band or below the valence band; use semiconductor with low bandgap; color center formation in band gap or alter the surface. Frequently, it is done by doping with metal and/or nonmetal; codoping with diverse combination of donor and acceptor materials; forming composites; sensitization or substitution [49].

Modification of TiO<sub>2</sub> such as forming nanocomposites with carbon nanotubes (CNTs), contributes to boosting of photocatalytic activity. CNTs are chemically inert, stable, with high specific surface and charge mobility [50]. A nanocomposite system of TiO<sub>2</sub>/CNT enables absorption of wider wavelengths due to formed C–O–Ti bonds [51]. It was noticed that increasing of CNT is proportional with the photocatalytic degradability of pollutants [52,53].

Even though suspended photocatalysts tend to be more reactive than immobilized, with appropriate design, mass and photon transfer limitations can be mastered [54]. The most suitable method used for synthesis of nanocomposites and its immobilization on inert carrier is the sol-gel method [51]. The method is considered as easy to use, does not require expensive equipment, and is non-destructive [55–57]. In current work, the mesh-like support was used to achieve a large and irregular photocatalytic layer by optimized sol-gel to overcome the mass and photon transfer limitations.

As a surface phenomenon, solar photocatalysis is highly dependent on the irradiation intensity. Hence, intensification of photocatalysis can be achieved not only by different photocatalyst's formulations, but also with an appropriate choice of reactor design and its usability of incident irradiation in reaction space. An optimal reactor, compound parabolic collector (CPC) reactor, is recommended [49,52] as state-of-the-art in design. Its application on a larger scale has been recognized as technically and economically feasible [58,59]. The usage varies from pilot scales to demonstration plants with collectors' surface areas from 3 to 150 m<sup>2</sup> [49].

Therefore, the aim of this work was to study the impact of solar photocatalysis intensification by using modified TiO<sub>2</sub>/CNT photocatalyst in comparison to TiO<sub>2</sub> usage. Immobilized photocatalysts were placed in an optimal CPC reactor configuration under an artificial source of solar containing UVA and UVB light. Four widely used compounds (DF, IMI, BT, MB) were used as study micropollutants. The developed mathematical model [52] was applied in order to calculate intrinsic reaction rate constants ( $k_i$ ) for studied micropollutants. In the model, the effect of the photocatalyst optical properties and incident irradiation under UVA and UVB light were defined, enabling the intrinsic reaction rate constant to be independent of the irradiation conditions and applied catalyst and applicable to other usage. Given settings enable the developed model to be effectively applied for different irradiation conditions.

## 2. Results and Discussion

### 2.1. Intensification by Photocatalyst Formulation

According to previous reporting in the paper [52], based on Micro-Raman spectroscopy results, indices of achieving the chemical bonds between composite TiO<sub>2</sub>/CNT on a glass fiber mesh were observed. Pure samples of MWCNT showed characteristic peaks and bands at 1340, 1580, and 2680 cm<sup>−1</sup>, while for TiO<sub>2</sub>, characteristic bands at 148, 286, 399, and

$633\text{ cm}^{-1}$ . In the composite sample of  $\text{TiO}_2/\text{CNT}$ , dominant bands were from  $\text{TiO}_2$  along with the affected MWCNT bands which in composite appeared at  $1290$  and  $1620\text{ cm}^{-1}$ . The indices about establishing chemical bonding between  $\text{TiO}_2$  and MWCNT on glass fibers were additionally confirmed by SEM results. At higher magnifications ( $200,000\times$ ), bonding of  $\text{TiO}_2$  and MWCNT was clearly noticeable, despite the uneven immobilization along the fiber that can be noticed as aggregates at  $1000\times$  magnifications (Figure 1).

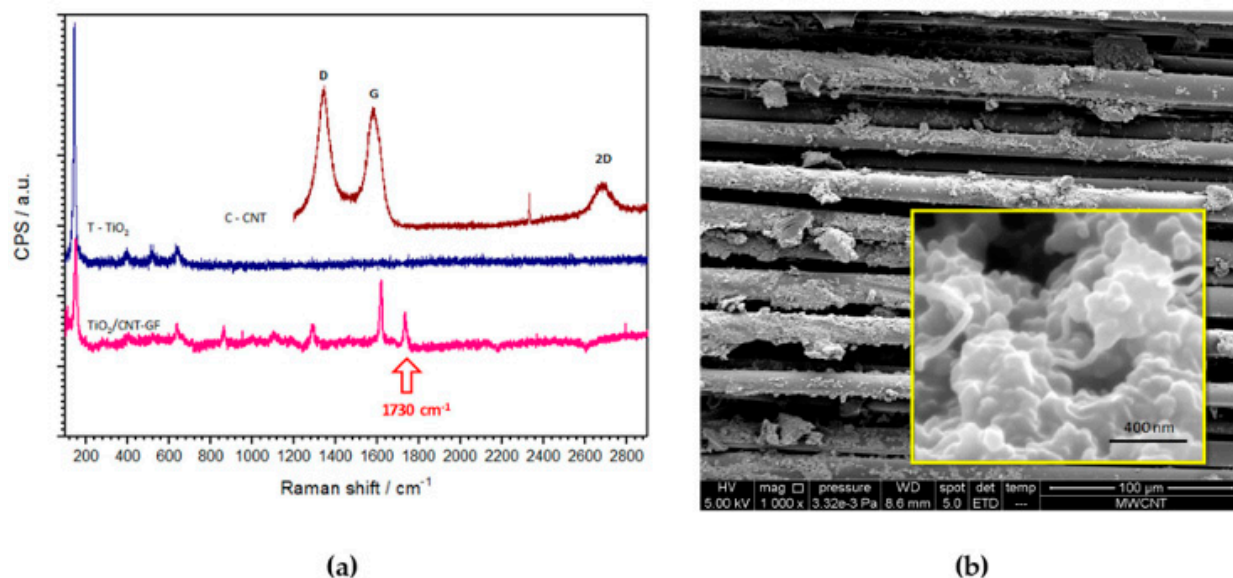


**Figure 1.** (a) Raman spectra of the photocatalytic constituents and composite film on glass fiber mesh; (b) SEM image of  $\text{TiO}_2/\text{CNT}$  at  $1000\times$  magnification and  $200,000\times$  (given as embedded figure) [52].

According to the DRS spectra (Figure 2), all photocatalytic film samples exhibit photo-absorption in the range between  $250$  and  $400\text{ nm}$ . To relatively enhance the absorption bands of different samples, the Kubelka–Munk function was applied, while the Tauc equation was applied to evaluate the type and extent of transition, along with the bandgap's extent. Therefore, while  $\text{TiO}_2$  is without a doubt a semiconducting material with indirect allowed transitions and bandgap value near the  $3.2\text{ eV}$ , the conventional calcium silicate glass, even though it is not a semiconducting material, may hinder or contribute to the semiconducting behavior of the composite with indirect allowed transitions and a bandgap value near the  $3.85\text{ eV}$ . On the other hand, MWCNT as a conducting material shows direct allowed transitions with bandgap value between  $2.9$  to  $3.6\text{ eV}$  depending on the treatment. For pure  $\text{TiO}_2$  and  $\text{TiO}_2$  immobilized on glass fibers, determined bandgap values were  $3.22$  and  $3.48\text{ eV}$ , respectively. When it comes to the composite  $\text{TiO}_2/\text{CNT}$ , an average bandgap value of  $3.12\text{ eV}$  can be expected while none of the transition types fully dominate. For example, if the  $\text{TiO}_2$  is governing the composite behavior, the calculated bandgap value is  $2.97\text{ eV}$ , while if the MWCNT is governing the composite behavior, the calculated bandgap value is  $3.27\text{ eV}$ . Observed values suggest that a considerable synergetic photocatalytic effect was achieved.

In a research study [60], aging of photocatalysts were tested. Results have showed that depending on the preparation of the  $\text{TiO}_2/\text{CNT}$  photocatalyst during the immobilization process, uneven dispersion can impact on the lower photocatalytic activity compared to  $\text{TiO}_2$ . Regarding the durability of  $\text{TiO}_2/\text{CNT}$  and  $\text{TiO}_2$  itself, it is observed that in a period of  $90$  days in water, photocatalyst's mass loss was  $6\%$  and  $11\%$  for  $\text{TiO}_2$  and  $\text{TiO}_2/\text{CNT}$ , respectively. Reduced photocatalytic activity is observed as well, however with the aging of photocatalysts on the air, improvements of photocatalytic activity are achieved.

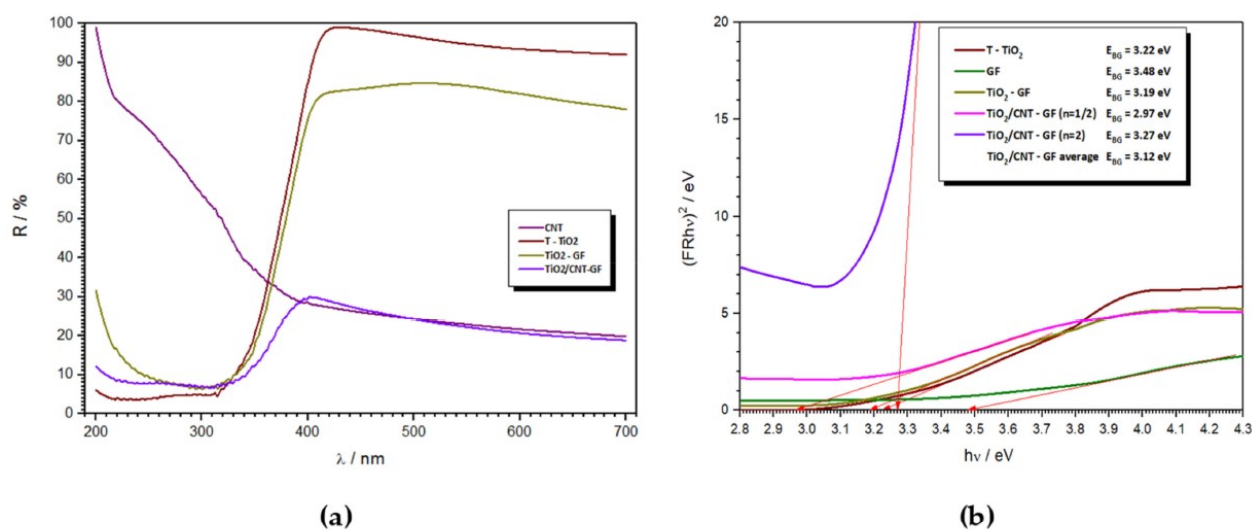


**Figure 2.** (a) DRS UV-vis spectra; (b) Tauc plot for the photocatalytic film constituents and photocatalytic composites on glass mesh [52].

## 2.2. Photolytic and Photocatalytic Degradation of Selected Pollutants

In order to discuss intensified degradation of selected pollutants, photolytic experiments were conducted under the same conditions as the photocatalytic one. Namely, once pollutants are in the environment, they are subjected to the photolysis. It is a process of chemical bond breakage due to photons absorption in an aqueous media initiated under the UV or visible irradiation spectra [5,61,62]. Its efficiency is impacted by the complexity of pollutant chemical structure and conditions in which experiments are conducted (models vs. real water samples). Therefore, photolysis alone, is usually not sufficient to achieve substantial effectiveness of pollutants' degradation [5].

However, the photolytic and photocatalytic degradation results were compared based on the assumption that degradation of selected pollutants follows the pseudo first-order kinetic model. According to the first-order kinetic model, basic kinetic Equation (1) with degradation rate  $k > 0$  and initial pollutant's concentration  $C(0) = C_0$  for time  $t = 0$  can be written as the following Equations (2) and (3) [63]:

$$r = k[X]^n \quad (1)$$

$$C(t) = C_0 e^{-kt} \quad (2)$$

$$\ln(C(t)) = \ln(C_0) - kt \quad (3)$$

where  $C(t)$  is concentration at time  $t$  (min),  $C_0$  is initial concentration and  $k$  is degradation rate constant ( $\text{min}^{-1}$ ).

Following the given Equations (2) and (3), degradation rate constants for photolysis, photocatalysis with TiO<sub>2</sub> and photocatalysis with TiO<sub>2</sub>/CNT were obtained. Results are graphically presented on Figure 3, and further discussed.

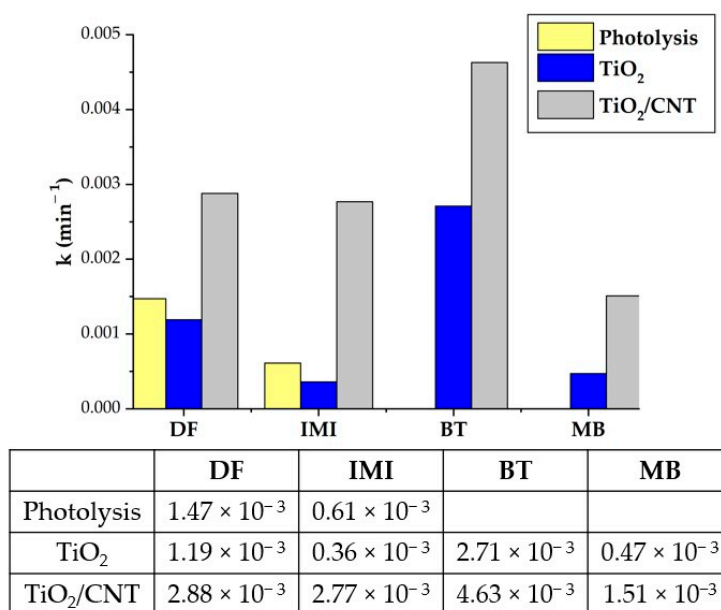


**Figure 3.** Photolytic and photocatalytic (TiO<sub>2</sub>, TiO<sub>2</sub>/CNT) degradation rate constants  $k$  (min<sup>-1</sup>) according to pseudo-first-order kinetic model for studied model pollutants (DF, IMI, BT, and MB).

Even though degradation of DF by hydroxyl radicals follows second-order kinetics, with approximation of steady-state concentration of hydroxyl radicals, reaction is usually treated as a pseudo-first-order kinetic model [7]. Furthermore, for highly diluted systems ( $C_0 < 10^{-3}$  M), the reaction can be considered pseudo-first order [64]. In this paper, as it can be seen on Figure 3, degradation rates of both photolysis ( $k_{DF} = 1.47 \times 10^{-3}$  min<sup>-1</sup>,  $R^2 = 0.99$ ) and photocatalysis ( $k_{DF,TiO_2} = 1.19 \times 10^{-3}$  min<sup>-1</sup>,  $R^2 = 0$ ;  $k_{DF,TiO_2/CNT} = 2.88 \times 10^{-3}$  min<sup>-1</sup>,  $R^2 = 0.99$ ) fit into pseudo-first order kinetic.

Furthermore, depending on experimental setup, photolytic degradation of DF can be described as negligible [45] or significantly better [2,7,65] in comparison with photocatalysis. In our study (Figure 3), photolytic degradation of DF is slightly better than photocatalytic degradation with TiO<sub>2</sub>. Similar observations were made previously [2,65]. However, authors in their studies had worked with suspended TiO<sub>2</sub> in different reactor setup and irradiation values; CPC under sunlight [65] and batch reactor with UV/Vis spectra lamp [2], respectively. Nevertheless, as it was stated in [65], since DF absorbs UV light ( $\lambda_{max} = 277$  nm), photolysis is a relevant process and it can be better than photocatalysis, thus, much less photons are available to generate electron-hole pairs due to interference with DF absorption of photons [2].

Regarding the photolysis studies in aqueous media, IMI has showed as readily degradable with a first-order rate kinetics [11,63]. As it can be seen on Figure 3, in this paper degradation rates of both photolysis ( $k_{IMI} = 6.1 \times 10^{-4}$  min<sup>-1</sup>,  $R^2 = 0.74$ ) and photocatalysis ( $k_{IMI,TiO_2} = 3.6 \times 10^{-4}$  min<sup>-1</sup>,  $R^2 = 0.87$ ;  $k_{IMI,TiO_2/CNT} = 2.77 \times 10^{-3}$  min<sup>-1</sup>,  $R^2 = 0.99$ ) fit into the first order kinetic. It can be noticed that photolytic degradation of IMI is slightly faster than the photocatalytic degradation by TiO<sub>2</sub>, even though the other way around would be expected. The same phenomenon was observed with DF photolytic and photocatalytic (by TiO<sub>2</sub>) degradation rates. Therefore, since most pesticides absorb UV light ( $\lambda_{IMI} = 277$  nm) [66], as well as formed intermediates [67], reduction of photons available to react with photocatalysts surface in reaction system occurs. As it was stated in the literature [11,63], different irradiation conditions in photolytic studies impact on the degradation rates of IMI. For instance, during the 2-h experiment under natural sunlight, 38% of IMI degradation was achieved [63]. On the other hand, 40-h were needed under UV lamps to achieve 95% of IMI degradation [11].

Although, BT is subjected to direct photolysis with first-order kinetic reaction mechanism under UV light [68], that was not the fact in our study. The most efficient degra-

dation of BT is in UVC spectra since maximum absorption is detected at  $\lambda_{BT} = 254$  nm, while in our study, experiments were done under lamps with UVA and UVB spectra. In their paper [68], authors have reported slow photolysis degradation under lamps with UVA and UVB light. However, DF and IMI absorb the UV light as well, but BT's relatively long persistence in the environment is due to the insensitivity to visible light [14]. Nevertheless, sunlight photolysis is a relevant process for BT degradation in surface waters [16] due to reaction with reactive transient species, though more toxic compounds can be formed if there is no mineralization [13]. In our study, BT photolysis was a negligible process as in [13], while photocatalysis were noticeable processes of degradation ( $k_{BT, TiO_2} = 2.71 \times 10^{-3} \text{ min}^{-1}$ ,  $R^2 = 0.97$ ;  $k_{BT, TiO_2/CNT} = 4.63 \times 10^{-3} \text{ min}^{-1}$ ,  $R^2 = 0.98$ ).

The lack of photolysis and slower photocatalytic degradation than expected by  $TiO_2$  can be explained due to the higher initial concentration ( $C_{0,MB} = 25$  ppm) used in experiments compared with literature ( $C_{0,MB} = 10$  ppm, [69]), as well as usage of  $TiO_2$  in suspension, while in our case immobilized  $TiO_2$  was used. However, in the study [70], photolysis of MB was as well reported as neglected, while photocatalysis with  $TiO_2$  P25 achieved 46% during three hours of experiment. In their work [69], degradation rate of  $3.4 \times 10^{-3} \text{ min}^{-1}$  was achieved with  $TiO_2$  P25 in suspension, while we have observed 10 times slower degradation rate  $k_{MB, TiO_2} = 4.7 \times 10^{-4} \text{ min}^{-1}$  ( $R^2 = 0.86$ ). However, similar degradation rate was observed when a composite of 1%-MWCNT/ $TiO_2$  was used;  $4.7 \times 10^{-3} \text{ min}^{-1}$  versus  $k_{MB, TiO_2/CNT} = 1.51 \times 10^{-3} \text{ min}^{-1}$  ( $R^2 = 0.98$ ). The slight difference value is attributed to the form of photocatalyst's usage.

### 2.2.1. Intensification of Photocatalytic Degradation

For all studied pollutants model solutions, equilibrium was established in 30 min (Figure 4). Additionally, adsorption on the surface of both photocatalysts was observed, but it was negligible. In consistence with literature findings, [2] adsorption of DF on both photocatalysts was not significant; 1% and 6% on  $TiO_2$  and  $TiO_2/CNT$ , respectively. Equilibrium was achieved during the 30 min in dark, and slightly higher adsorption (+5%) was observed with  $TiO_2/CNT$  photocatalyst. In the literature [66,71] during the 30 min of dark experiment, adsorption of IMI was negligible. However, in our study, 13% and 20% of adsorption on  $TiO_2$  and  $TiO_2/CNT$  was observed, respectively. It was reported [67] that concentrations of IMI higher than 20 ppm inhibit the photocatalysis due to high adsorption rate of IMI on the photocatalyst's surface. Since in our study initial concentration was lower than stated ( $C_0 = 10$  ppm), equilibrium was achieved. However, occupied sites on the photocatalysts surface by adsorbed IMI molecules could slow down the photocatalysis by  $TiO_2$ . In their work [69], when adsorption tests of MB on pure MWCNTs was conducted, strong adsorption capacity was noticed, 100% of MB adsorption was noticed during the 120 min. Nonetheless, despite adsorption,  $TiO_2$  composites with CNT exhibit increased photocatalytic activity under visible light, and degrade MB more efficiently due to a simultaneous increase of active specific surface. In this study, 4% and 11% of MB adsorption on  $TiO_2$  and  $TiO_2/CNT$  was observed, respectively. When it comes to BT adsorption, it was negligible, where 2% and 4% for  $TiO_2$  and  $TiO_2/CNT$  were observed, respectively. Though, it was reported [72] that MWCNT can be used as a sorbent in solid phase extraction, and successfully used as a pretreatment to pre-concentrate BTs from real water samples.

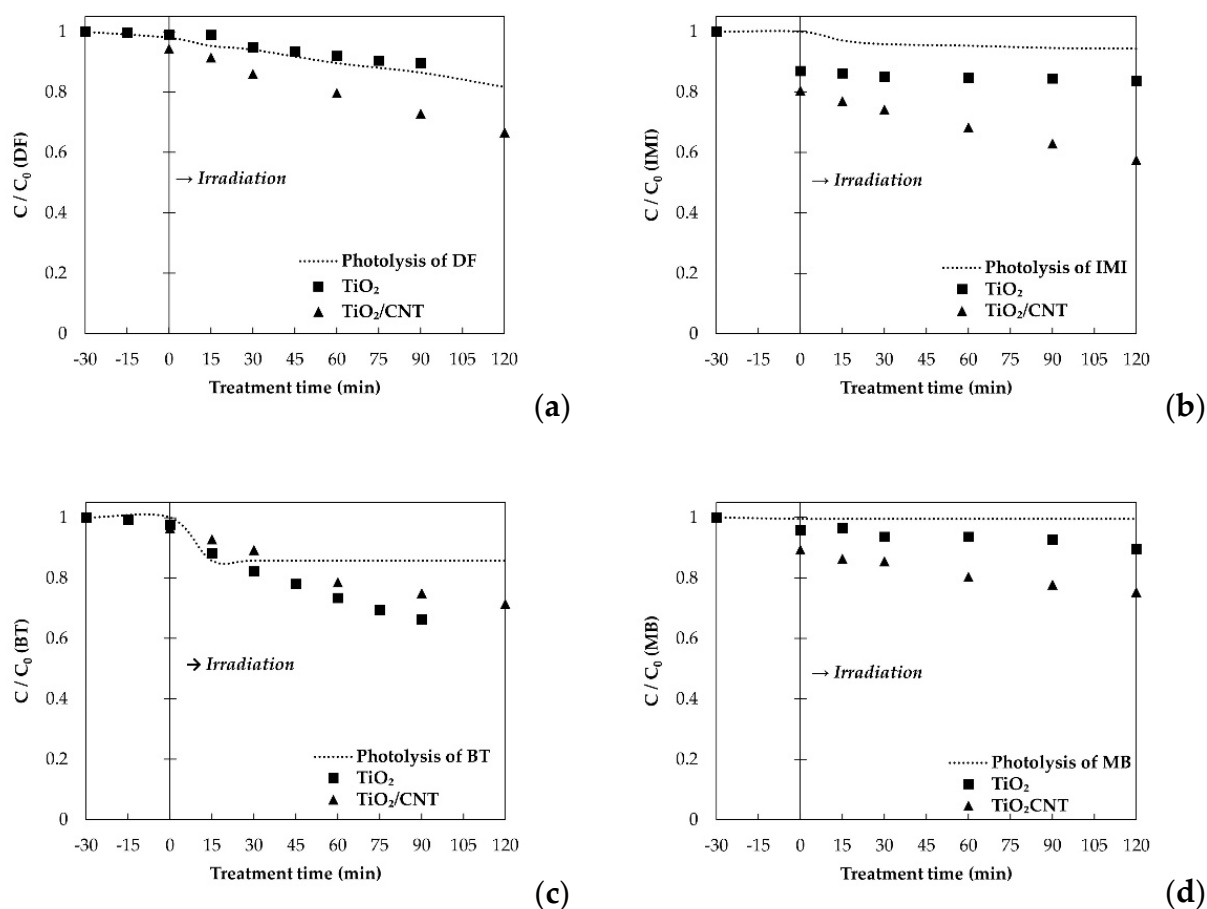


**Figure 4.** Experimental results of photolytic and photocatalytic degradation on TiO<sub>2</sub> and TiO<sub>2</sub>/CNT of: (a) diclofenac (DF), (b) imidacloprid (IMI), (c) 1H-benzotriazole (BT), (d) methylene blue (MB). Presented results are obtained during the dark and irradiated experiments.

During the degradation process, to avoid formation of toxic derivatives, an optimal treatment time is crucial to define. For instance, in the study [45], after 120 min of DF photocatalytic degradation, toxicity was not observed despite the formation of derivatives as chloro and hydroxyl phenols radicals. Photolytic DF degradation rate of 28% was achieved in 4 h when demineralized water was used, while in the same time, 36% was achieved when fresh water was used [65], confirming that the presence of other compounds which can react as radicals contribute to the photolysis of DF [3]. In our study, during the 120 min, 17% of DF degradation was achieved. At the same time, by TiO<sub>2</sub> photocatalysis 10% and TiO<sub>2</sub>/CNT 29% of DF degradation was achieved, respectively.

Even though in literature [9] 53.6% of DF degradation rate was achieved, the study was with TiO<sub>2</sub> in suspension. This confirms that the presence of DF molecules in the solution scavenge photons on their way to the immobilized photocatalysts surface. In systems with suspended photocatalysts, given phenomena is reduced due to the suspension form. It was reported that a vital role in DF degradation plays the concentration of dissolved oxygen [2], even though hydroxyl radicals have an important effect on the DF degradation as well [9].

The intensification of DF degradation by TiO<sub>2</sub>/CNT photocatalysts in comparison with TiO<sub>2</sub> was observed in our study. For example, in their paper [2], the authors did not obtain significant photocatalytic degradation when composites of 10:100 (*w/w*) MWCNT<sub>ox</sub> and TiO<sub>2</sub> (anatase) were used. In their previous work [73], authors had given possible explanations, one of which is inhibition of electron–hole generation by interaction of TiO<sub>2</sub> and CNT. The stated does not apply to our study, since our experiments were conducted with immobilized photocatalysts, preventing interaction between nanoparticles, yet intensifying radicals' generation necessary for DF degradation.

Previous results [66] have demonstrated effective (68%) photocatalytic degradation of IMI by immobilized TiO<sub>2</sub> on a glass plate under the UVC irradiation in 180 min. It was observed that photocatalytic degradation by TiO<sub>2</sub> in batch reactors under UVA light is a relatively slow process as was the case with findings in our study. Photocatalytic degradation of IMI under UVA and UVB light by TiO<sub>2</sub> was 4%, however, by TiO<sub>2</sub> modification with CNT, IMI degradation increases to 29%.

The Intensification of IMI degradation by composites of TiO<sub>2</sub> and CNT was reported by [71]. During the 30-min dark experiments, a small increase in adsorption was observed, which had stabilized in given time. Under UV light, 32% and 53% IMI removal was achieved by TiO<sub>2</sub> and TiO<sub>2</sub>/CNT photocatalysis in 3 h, respectively. Addition of CNT contributes to Ti-O-C bond formation, thus allowing the induction of e<sup>-</sup> by photons to migrate into CNT and diminishing charge recombination, while e<sup>-</sup> can attack H<sub>2</sub>O to form hydroxyl radicals.

Consequently, usage of irradiated semiconductors has gained on the importance in the BT removal research. In their research [13], authors used TiO<sub>2</sub> in suspension form and demonstrated rapid removal of BT without formation of toxic byproducts. They proposed that any other AOP that use hydroxyl radicals as the main oxidants might be useful for BT removal. In our study, 32% of BT was degraded within 120 min by TiO<sub>2</sub>. However, intensification of BT photocatalytic degradation by modification with CNT was not observed, only 26% BT removal was achieved. A similar trend was observed in the studies [73,74] where carbamazepine and DF photocatalytic degradation by TiO<sub>2</sub> and TiO<sub>2</sub>/CNT were studied. Two hypotheses were offered; (1) high electrical conductivity of CNTs supplies TiO<sub>2</sub> with electrons and reduces separation of electron-hole pairs; (2) CNTs are excited to produce electron-hole pairs which are annihilating production of TiO<sub>2</sub> electron-hole pairs generation when conduction band of CNTs is higher than that of TiO<sub>2</sub>.

Regarding the MB degradation, it has been reported [33] that about 80% of MB could be degraded under UVB light irradiation in 120 min, while in 60 min 90% of MB could be degraded under sunlight irradiation when immobilized TiO<sub>2</sub> was used. A higher removal rate of MB with suspended TiO<sub>2</sub> (47% in 180 min) was observed by [69]. However, only 6% of MB in 120 min by TiO<sub>2</sub> was degraded in our case. The lower removal efficiency of MB with TiO<sub>2</sub> was observed as well by [55], 13% in 100 min. Nonetheless, intensification of MB degradation when CNT were employed has been noticed. During the 180 min, 61.9% removal rate of MB was obtained with 1%-MWCNT/TiO<sub>2</sub> [14], while 76% of MB was degraded in 100 min by MWCNT:TiO<sub>2</sub> = 1:3 (*w/w*) [55]. In our study, immobilized TiO<sub>2</sub>/CNT (10:1, *w/w*) was employed and 16% removal rate was observed.

## 2.2.2. Modeling of Photocatalytic Degradation

Concerning more detailed analysis of photocatalytic degradation, especially by TiO<sub>2</sub> modification with CNT, mathematical modeling with defined intrinsic parameters was applied. Description of model developing is given later in the text. Intrinsic degradation rate constants  $k_i$ , as well as intensification factors  $Y_{cat}$  for the studied pollutants were obtained and given in Table 1.

**Table 1.** Intrinsic degradation rate constants for DF, MI, BT and MB along with the intensification factors due to TiO<sub>2</sub> modification with CNT.

	$K_i$ ( $s^{-1}W^{-0.5}m^{1.5}$ )	$Y_{cat}$ (-)
DF	$3.56 \times 10^{-10}$	2.35
IMI	$8.90 \times 10^{-11}$	8.84
BT	$1.20 \times 10^{-09}$	0.64
MB	$1.62 \times 10^{-10}$	2.52

Photocatalytic degradation of studied pollutants modeled based on parameters given in Table 1, fit well with the experimental data as it can be seen in Figure 5. As it was already

discussed, intensification of DF, IMI, and MB photocatalytic degradation was observed which can be noticed by the value of  $Y_{cat} > 1$ . The highest intensification contribution to a pollutant's degradation in comparison with  $TiO_2$  can be given in the following order IMI (8.84) < MB (2.52) < DF (2.35). On the other hand, intensification of BT degradation by photocatalyst's modification was not observed and therefore value of  $Y_{cat} < 1$ .

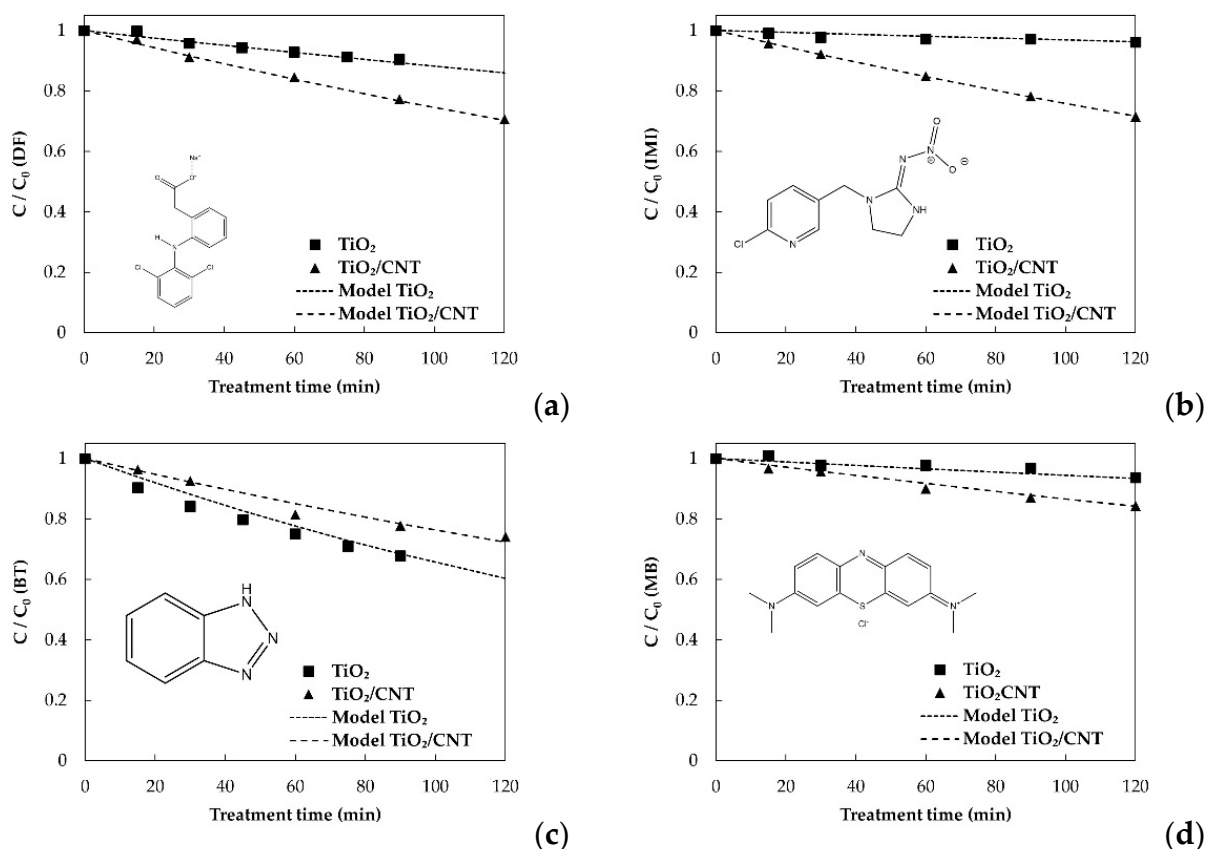


**Figure 5.** Photocatalytic degradation on  $TiO_2$  and  $TiO_2/CNT$  of: (a) diclofenac (DF), (b) imidacloprid (IMI), (c) 1H-benzotriazole (BT), (d) methylene blue (MB). Fitting of mathematical modelling results along with the obtained experimental data.

Furthermore, by using a modeling approach, it is possible to predict time necessary for the pollutant's degradation. For instance, 90% of DF and BT degradation is possible to achieve within one day (Figure 6a,c), while degradation of IMI and MB depends on the used photocatalysts (Figure 6b,d). More elaborate data about the time degradation can be found in Table 2.

**Table 2.** Overview of time necessary to achieve 50% and 90% of efficient photocatalytic degradation for studied pollutants. Results are obtained based on developed model prediction.

	$TiO_2$				$TiO_2/CNT$			
	DF	IMI	BT	MB	DF	IMI	BT	MB
50%	9 h	37 h	3 h	21 h	4 h	4 h	4 h	8 h
90%	31 h	>84 h	9 h	67 h	13 h	14 h	15 h	27 h

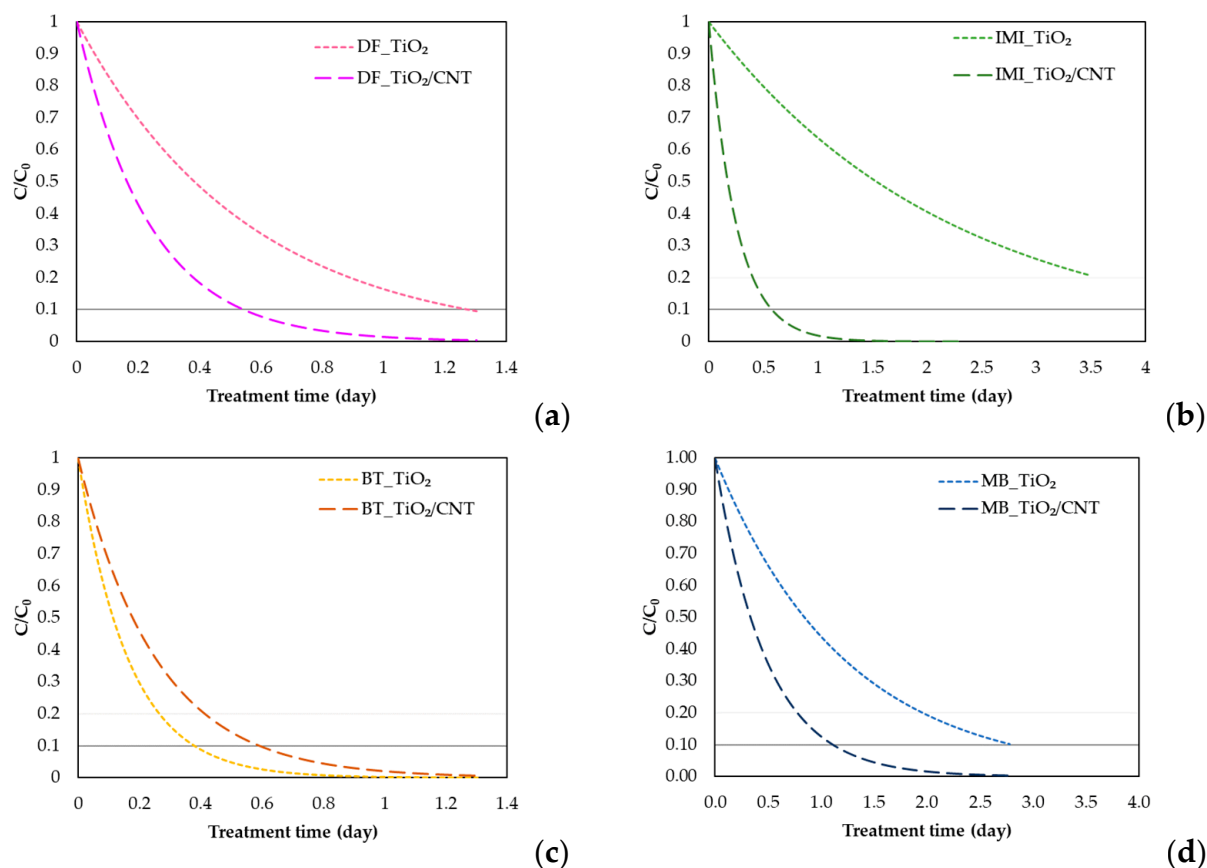


**Figure 6.** Modeled photocatalytic degradation on  $TiO_2$  and  $TiO_2/CNT$  over period of time to achieve 90% efficiency of: (a) diclofenac (DF), (b) imidacloprid (IMI), (c) 1H-benzotriazole (BT), (d) methylene blue (MB).

### 3. Materials and Methods

#### 3.1. Model Pollutants

In this work, photocatalytic degradation of 1H-benzotriazole (BT; 99%, Acros Organics, NJ, USA), imidacloprid (IMI; p.a., Sigma-Aldrich Chemie GmbH, Steinheim, Germany), and diclofenac (DF; p.a., Sigma-Aldrich Chemie GmbH, Steinheim, Germany) were studied. As a reference measurement, photocatalytic degradation of methylene blue (MB; VWR International, Leuven, Belgium) was studied as well. Model solutions were prepared with initial concentrations as follows:  $C_0(BT) = 5$  ppm,  $C_0(IMI) = 5$  ppm,  $C_0(DF) = 10$  ppm and  $C_0(MB) = 25$  ppm in accordance with the literature findings [7,67,75].

Concentrations of IMI and DF were determined by high-performance liquid chromatography (HPLC-UV, Agilent Technologies 1200 Series, Santa Clara, CA, USA). A mixture of 0.1% of formic acid and methanol was used as a mobile phase along with the flow rate 0.5 mL/min and 0.3 mL/min for IMI and DF, respectively. Detection was at 254 [76] and 258 nm, respectively [77].

Decrease of concentrations of BT and MB were determined by UV-Vis spectrophotometry (Avantes AvaLight-DH-S-Bal Spectrometer, Lafayette, USA) at 256 nm [78] and 660 nm [39,43,44,79–81], respectively. Regarding the MB, visible photodecolorization was observed as a result of degradation.

#### 3.2. Photocatalysts Preparation

In the experiments, two photocatalysts were used: commercial  $TiO_2$  (Evonik Operations GmbH, Aeroxide<sup>®</sup>  $TiO_2$  P25, Hanau-Wolfgang, Germany, 30 nm, 56 m<sup>2</sup>/g, 75:25 anatase to rutile mass ratio) and  $TiO_2/CNT$ , a mixture of  $TiO_2$  and CNT (MWCNT, Sigma-Aldrich Chemie GmbH, Steinheim, Germany, 50–90 nm, >95% carbon) in a ratio of 10:1

(*w:w*) (Figure 7). Both photocatalysts were immobilized on a glass fiber mesh (Keltex, Karlovac, Croatia, density 480 g/m<sup>2</sup>) of defined dimensions (480 × 250 mm) by modified sol-gel procedure [52]. According to the procedure, photocatalyst (TiO<sub>2</sub> or TiO<sub>2</sub>/CNT) is added in a solution of distilled water and ethanol (p.a. 96%) with volume ratio 1:1 and stirred for 15 min during which the pH is adjusted to 1.5 with the addition of acetic acid (Kemika, Zagreb, Croatia). Homogenization of solution is then performed by ultrasonic probe for 2 min (30 W, 20 kHz). After sonication, tetraetoxysilane (TEOS) was added and immobilization solution was stirred for 1 h at 50 °C. Meanwhile, glass fiber mesh was cut to prepare supports for the immobilization. Supports were cleaned with ethanol, treated for 5 min with 10 M NaOH and rinsed with deionized water. Pretreated supports were 4 times in a row dipped in immobilization solution and then dried at 70 °C for 30 min. The immobilization procedure was finished after an additional week of immobilized photocatalysts drying at room temperature.



**Figure 7.** The image of photocatalysts: (a) TiO<sub>2</sub> photocatalytic film on glass fiber mesh, (b) TiO<sub>2</sub>/CNT photocatalytic film on glass fiber mesh.

Characterization was performed by using Raman spectroscopy (HORIBA Jobin Yvone T64000 spectrometer, Bensheim, Germany) with a 532.5 nm, solid-state laser excitation); the scanning electron microscopy (FEG SEM Quanta250 FEI microscope, Hillsboro, Oregon, USA) and diffuse reflectance spectroscopy (DRS, Perkin-Elmer Lambda 35, Waltham, MA, USA). Additional information were described in more details in our previous paper [52].

### 3.3. Reaction Set Up

The experiments were performed in a compound parabolic collector (CPC) reactor (Figure 8) which represents state-of-the-art in reactor design. The CPC reactor set up consists of two parallel quartz tubes ( $L = 50$  cm,  $D_{\text{outer}} = 3$  cm,  $D_{\text{inner}} = 2.7$  cm) connected with a PTFE U-tube of the same inner dimension to avoid changes in flows rates. Quartz tubes are placed in a compound parabolic mirror made of highly reflective alumina (JBL, Neuhofen, Germany, Solar Reflect 50).

As an irradiation source, a custom-made panel with three full spectra lamps (JBL, Neuhofen, Germany, Solar Ultra linear fluorescent lamps: Color, Tropic and Nature, T5, 145 cm, nominal power 80 W) and corresponding reflective mirrors (JBL, Neuhofen, Germany, Solar Reflect 146) was used. The UVB and UVA intensities were determined at the lamp wall ( $I_w$ ) by UVX radiometer (UVP Products, Analytik Jena US LLC, Upland, CA) fitted with corresponding longwave UV-A UVX-36 (range 335–385 nm) and midrange UV-B UVX-31 (range 280–340 nm) sensors of  $\pm 5\%$  accuracy (Figure 9). The CPC reactor was inclined at 12° in correspondence with the inclination of a custom-made panel which was set up at 10 cm above the reactor.

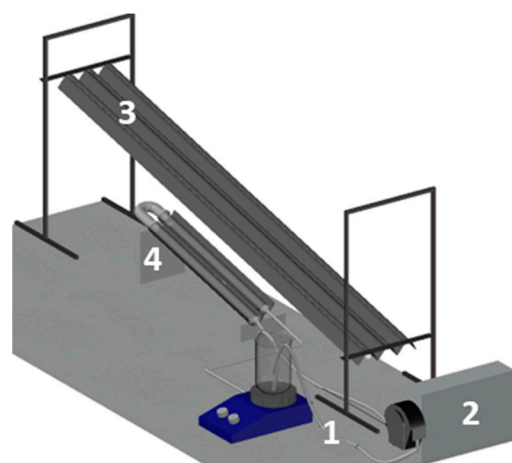


**Figure 8.** The set up for the CPC reactor. (1) Solution mixing and sampling; (2) Peristaltic pump; (3) Irradiation source; (4) CPC reactor.

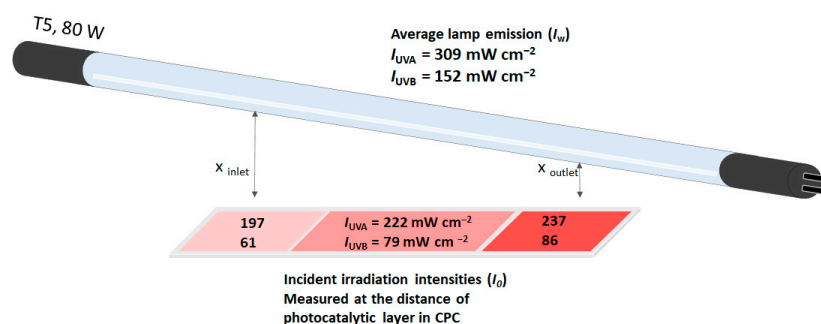


**Figure 9.** Average incident irradiation intensities on photocatalyst surface in CPC regarding lamps' positioning.

The CPC reactor was attached to a beaker of work volume 1.5 L with silicone tubes and peristaltic pump (Masterflex®) of workflow  $26.5 \text{ cm}^3/\text{s}$ . The volume of CPC reactor with the tubes was 0.5 L. The beaker was placed on the magnetic stirrer in order to maintain the equilibrium in the solution. The CPC reactor was connected to the beaker in recirculation with the silicone tubes.

For the purposes of research, photolysis and photocatalysis experiments were conducted following the same methodology for all the model solutions. To achieve sorption equilibrium, the model solution was first recirculated for 30 min without irradiation. In the next 120 min, photolysis and photocatalysis were measured. To estimate the adsorption of model pollutants on the photocatalytic films, control experiments were conducted in 'dark' in the full length of 120 min. All experiments were conducted three times and average values were reported.

### 3.4. Mathematical Modeling of Intensification Factors

Determination of differences in the degradation rates of model pollutants due to different photocatalytic films requires proper modeling of kinetics parameters.

The basic kinetic Equation (1) was modified into Equation (4) to incorporate intrinsic parameters related with the photocatalytic degradation of selected pollutants over irradiated  $\text{TiO}_2$  film.

$$r_i = -k_i((\mu I_0(L, W))_{UVB} + (\mu I_0(L, W))_{UVA})^m [X]^n \quad (4)$$

The  $\mu(\text{m}^{-1})$  stands for the absorption coefficient averaged over the spectrum of incident irradiation (in UVB and UVA region), while the  $I_0(L, W)$  ( $\text{W m}^{-2}$ ) stands for the incident photon flux at the film surface along its length, and  $m$  is the order of reaction with

respect to irradiation absorption. By introducing the  $(\mu I_0(L, W))^m$  into the kinetic model, resulting reaction rate constants became independent of irradiation condition and applied catalysts [82]. Therefore,  $k_i$  stands for the intrinsic degradation rate constant of selected pollutant ( $i$ ).

By introducing the intensification index,  $Y_{cat}$ , Equation (4) was modified into Equation (5):

$$r_i = -k_i Y_{cat} ((\mu I_0(L, W))_{UVB} + (\mu I_0(L, W))_{UVA})^m [X]^n \quad (5)$$

The  $Y_{cat}$  assumes the enhancement in light absorption by photocatalysts, both in the UVA and UVB region but also in the visible part of applied irradiation. It can be used for facile determination of total intensification for new and improved photocatalyst formulations.

The reaction kinetic model was further combined with the material balance for plug flow reactor in recirculation. The Reynolds number was estimated using the hydraulic diameter equal to the wetted perimeter and for maintained flow in CPC was 134.8. Despite the laminar flow, average velocity was used neglecting the radial and axial differences in the velocity profile. The averaged fluid velocity was estimated at  $v = 4.99 \times 10^{-2}$  m/s in CPC, which was used in all related models. In CPC, outlet flow mixed with the reaction mixture in the recirculation tank led to different inlet concentrations in different reaction times. Material balance is given for the perfectly mixed reservoir tank:

$$V_{tank} \frac{d[X_i]_{tank}^{out}}{dt} = Q ([X_i]_{tank}^{in} - [X_i]_{tank}^{out}) \quad (6)$$

where

$$v \frac{d[X_i]}{dL} = r_i(L, t) \quad (7)$$

The numerical simulation was performed dividing the reaction space along the length and width—i.e., L and W directions—in sufficiently small intervals. A small-time increment ( $\Delta t$ ) equal to the reactor space time ( $\tau = V_R/Q$ ) was introduced. The material balance in the reactor was solved at time  $t$ . The time step counter was increased, and the procedure repeated. All simulations were performed in VBA module (Excel). Reaction rate constants ( $k_i$ ,  $s^{-1}W^{-0.5}m^{1.5}$ ) were determined by the trial-and-error method fitting the experimental values into the model by minimizing the variance.

#### 4. Conclusions

Photocatalytic degradation of DF, IMI, BT, and MB by immobilized  $TiO_2$  and  $TiO_2/CNT$  photocatalysts were achieved. Mathematical modelling which included mass transfer and photon absorption was applied and intrinsic reaction rate constants were estimated:  $k_{DF} = 3.56 \times 10^{-10} s^{-1} W^{-0.5} m^{1.5}$ ,  $k_{IMI} = 8.90 \times 10^{-11} s^{-1} W^{-0.5} m^{1.5}$ ,  $k_{BT} = 1.20 \times 10^{-9} s^{-1} W^{-0.5} m^{1.5}$ ,  $k_{MB} = 1.62 \times 10^{-10} s^{-1} W^{-0.5} m^{1.5}$ . In comparison with  $TiO_2$  photocatalysis, intensification of photocatalysis by  $TiO_2/CNT$  was observed for DF (10% to 29%), IMI (4% to 29%) and MB (6% to 16%), while that was not the case for BT (32% vs. 26%). Applied mathematical kinetic models can be effectively applied for different irradiation conditions which makes it extremely versatile and adaptable when predicting the degradation extents throughout the year using sunlight as the energy source at any location.

**Author Contributions:** Conceptualization, L.R., J.M. and I.G.; methodology, L.R. and J.M.; formal analysis, L.R.; investigation, L.R. and J.M.; resources, L.R.; writing—original draft preparation, L.R. and J.M.; writing—review and editing, I.G., I.B. and T.Č.; visualization, J.M.; supervision, I.G.; project administration, I.G.; funding acquisition, I.G. All authors have read and agreed to the published version of the manuscript.

**Funding:** This work has been supported by the following projects “Waste & Sun for photocatalytic degradation of micropollutants in water” (OS-Mi), supported by European Regional Development Fund, KK.01.1.1.04.0006. and “PV-WALL” PZS-2019-02-1555 in the Research Cooperability Program of the Croatian Science Foundation funded by the European Union from the European Social Fund under the Operational Program Efficient Human Resources 2014–2020.

**Data Availability Statement:** Not applicable.

**Acknowledgments:** Special thanks to project VIRTULAB—Integrated laboratory for primary and secondary raw materials for the equipment usage supported by European Regional Development Fund KK.01.1.1.02.0022.

**Conflicts of Interest:** The authors declare no conflict of interest.

## References

1. Ameta, R.; Solanki, M.S.; Benjamin, S.; Ameta, S.C. Photocatalysis. In *Advanced Oxidation Processes for Waste Water Treatment*; Elsevier: Amsterdam, The Netherlands, 2018; pp. 135–175, ISBN 9780128105252.
2. Martínez, C.; Canle, L.M.; Fernández, M.I.; Santaballa, J.A.; Faria, J. Aqueous degradation of diclofenac by heterogeneous photocatalysis using nanostructured materials. *Appl. Catal. B Environ.* **2011**, *107*, 110–118. [[CrossRef](#)]
3. Ribeiro, A.R.L.; Moreira, N.F.F.; Puma, G.L.; Silva, A.M.T. Impact of water matrix on the removal of micropollutants by advanced oxidation technologies. *Chem. Eng. J.* **2019**, *363*, 155–173. [[CrossRef](#)]
4. Kosek, K.; Luczkiewicz, A.; Fudala-Książek, S.; Jankowska, K.; Szopińska, M.; Svahn, O.; Tränckner, J.; Kaiser, A.; Langas, V.; Björklund, E. Implementation of advanced micropollutants removal technologies in wastewater treatment plants (WWTPs)—Examples and challenges based on selected EU countries. *Environ. Sci. Policy* **2020**, *112*, 213–226. [[CrossRef](#)]
5. Bustos, E.B.; Sandoval-González, A.; Martínez-Sánchez, C. Detection and Treatment of Persistent Pollutants in Water: General Review of Pharmaceutical Products. *ChemElectroChem* **2022**, *9*, e202200188. [[CrossRef](#)]
6. Espíndola, J.C.; Vilar, V.J.P. Innovative light-driven chemical/catalytic reactors towards contaminants of emerging concern mitigation: A review. *Chem. Eng. J.* **2020**, *394*, 124865. [[CrossRef](#)]
7. Arany, E.; Láng, J.; Somogyvári, D.; Láng, O.; Alapi, T.; Ilisz, I.; Gajda-Schrantz, K.; Dombi, A.; Kőhidai, L.; Hernádi, K. Vacuum ultraviolet photolysis of diclofenac and the effects of its treated aqueous solutions on the proliferation and migratory responses of *Tetrahymena pyriformis*. *Sci. Total Environ.* **2014**, *468–469*, 996–1006. [[CrossRef](#)] [[PubMed](#)]
8. Bi, L.; Chen, Z.; Li, L.; Kang, J.; Zhao, S.; Wang, B.; Yan, P.; Li, Y.; Zhang, X.; Shen, J. Selective adsorption and enhanced photodegradation of diclofenac in water by molecularly imprinted TiO<sub>2</sub>. *J. Hazard. Mater.* **2021**, *407*, 124759. [[CrossRef](#)]
9. Diaz-Angulo, J.; Porras, J.; Mueses, M.; Torres-Palma, R.A.; Hernandez-Ramirez, A.; Machuca-Martinez, F. Coupling of heterogeneous photocatalysis and photosensitized oxidation for diclofenac degradation: Role of the oxidant species. *J. Photochem. Photobiol. A Chem.* **2019**, *383*, 112015. [[CrossRef](#)]
10. Náfrádi, M.; Hlogyik, T.; Farkas, L.; Alapi, T. Comparison of the heterogeneous photocatalysis of imidacloprid and thiacloprid—reaction mechanism, ecotoxicity, and the effect of matrices. *J. Environ. Chem. Eng.* **2021**, *9*, 106684. [[CrossRef](#)]
11. Ding, T.; Jacobs, D.; Lavine, B.K. Liquid chromatography-mass spectrometry identification of imidacloprid photolysis products. *Microchem. J.* **2011**, *99*, 535–541. [[CrossRef](#)]
12. Mikolić, A.; Karačonji, I.B. Imidacloprid as reproductive toxicant and endocrine disruptor: Investigations in laboratory animals. *Arch. Ind. Hyg. Toxicol.* **2018**, *69*, 103–108. [[CrossRef](#)] [[PubMed](#)]
13. Minella, M.; De Laurentiis, E.; Pellegrino, F.; Prozzi, M.; Dal Bello, F.; Maurino, V.; Minero, C. Photocatalytic Transformations of 1H-Benzotriazole and Benzotriazole Derivates. *Nanomaterials* **2020**, *10*, 1835. [[CrossRef](#)] [[PubMed](#)]
14. Shi, Z.-Q.; Liu, Y.-S.; Xiong, Q.; Cai, W.-W.; Ying, G.-G. Occurrence, toxicity and transformation of six typical benzotriazoles in the environment: A review. *Sci. Total Environ.* **2019**, *661*, 407–421. [[CrossRef](#)] [[PubMed](#)]
15. Lee, J.-E.; Kim, M.-K.; Lee, J.-Y.; Lee, Y.-M.; Zoh, K.-D. Degradation kinetics and pathway of 1H-benzotriazole during UV/chlorination process. *Chem. Eng. J.* **2019**, *359*, 1502–1508. [[CrossRef](#)]
16. Weidauer, C.; Davis, C.; Raeke, J.; Seiwert, B.; Reemtsma, T. Sunlight photolysis of benzotriazoles—Identification of transformation products and pathways. *Chemosphere* **2016**, *154*, 416–424. [[CrossRef](#)] [[PubMed](#)]
17. Bahnmüller, S.; Loi, C.H.; Linge, K.L.; von Gunten, U.; Canonica, S. Degradation rates of benzotriazoles and benzothiazoles under UV-C irradiation and the advanced oxidation process UV/H<sub>2</sub>O<sub>2</sub>. *Water Res.* **2015**, *74*, 143–154. [[CrossRef](#)] [[PubMed](#)]
18. Reemtsma, T.; Miehe, U.; Duennbier, U.; Jekel, M. Polar pollutants in municipal wastewater and the water cycle: Occurrence and removal of benzotriazoles. *Water Res.* **2010**, *44*, 596–604. [[CrossRef](#)]
19. Dai, Q.; Chen, W.; Luo, J.; Luo, X. Abatement kinetics of highly concentrated 1H-Benzotriazole in aqueous solution by ozonation. *Sep. Purif. Technol.* **2017**, *183*, 327–332. [[CrossRef](#)]
20. Alotaibi, M.D.; McKinley, A.J.; Patterson, B.M.; Reeder, A.Y. Benzotriazoles in the Aquatic Environment: A Review of Their Occurrence, Toxicity, Degradation and Analysis. *Water Air Soil Pollut.* **2015**, *226*, 226. [[CrossRef](#)]
21. Yin, W.; Shao, H.; Huo, Z.; Wang, S.; Zou, Q.; Xu, G. Degradation of anticorrosive agent benzotriazole by electron beam irradiation: Mechanisms, degradation pathway and toxicological analysis. *Chemosphere* **2022**, *287*, 132133. [[CrossRef](#)]

22. Cancilla, D.A.; Martinez, J.; van Aggelen, G.C. Detection of Aircraft Deicing/Antiicing Fluid Additives in a Perched Water Monitoring Well at an International Airport. *Environ. Sci. Technol.* **1998**, *32*, 3834–3835. [[CrossRef](#)]
23. Loos, R.; Locoro, G.; Comero, S.; Contini, S.; Schwesig, D.; Werres, F.; Balsaa, P.; Gans, O.; Weiss, S.; Blaha, L.; et al. Pan-European survey on the occurrence of selected polar organic persistent pollutants in ground water. *Water Res.* **2010**, *44*, 4115–4126. [[CrossRef](#)] [[PubMed](#)]
24. Loos, R.; Tavazzi, S.; Mariani, G.; Suurkuusk, G.; Paracchini, B.; Umlauf, G. Analysis of emerging organic contaminants in water, fish and suspended particulate matter (SPM) in the Joint Danube Survey using solid-phase extraction followed by UHPLC-MS-MS and GC-MS analysis. *Sci. Total Environ.* **2017**, *607–608*, 1201–1212. [[CrossRef](#)]
25. LeFevre, G.H.; Müller, C.E.; Li, R.J.; Luthy, R.G.; Sattely, E.S. Rapid Phytotransformation of Benzotriazole Generates Synthetic Tryptophan and Auxin Analogs in Arabidopsis. *Environ. Sci. Technol.* **2015**, *49*, 10959–10968. [[CrossRef](#)] [[PubMed](#)]
26. LeFevre, G.H.; Lipsky, A.; Hyland, K.C.; Blaine, A.C.; Higgins, C.P.; Luthy, R.G. Benzotriazole (BT) and BT plant metabolites in crops irrigated with recycled water. *Environ. Sci. Water Res. Technol.* **2017**, *3*, 213–223. [[CrossRef](#)]
27. Yao, L.; Zhao, J.-L.; Liu, Y.-S.; Yang, Y.-Y.; Liu, W.-R.; Ying, G.-G. Simultaneous determination of 24 personal care products in fish muscle and liver tissues using QuEChERS extraction coupled with ultra pressure liquid chromatography-tandem mass spectrometry and gas chromatography-mass spectrometer analyses. *Anal. Bioanal. Chem.* **2016**, *408*, 8177–8193. [[CrossRef](#)]
28. Yao, L.; Lv, Y.-Z.; Zhang, L.-J.; Liu, W.-R.; Zhao, J.-L.; Liu, Y.-S.; Zhang, Q.-Q.; Ying, G.-G. Determination of 24 personal care products in fish bile using hybrid solvent precipitation and dispersive solid phase extraction cleanup with ultrahigh performance liquid chromatography-tandem mass spectrometry and gas chromatography-mass spectrometry. *J. Chromatogr. A* **2018**, *1551*, 29–40. [[CrossRef](#)]
29. Yao, L.; Zhao, J.-L.; Liu, Y.-S.; Zhang, Q.-Q.; Jiang, Y.-X.; Liu, S.; Liu, W.-R.; Yang, Y.-Y.; Ying, G.-G. Personal care products in wild fish in two main Chinese rivers: Bioaccumulation potential and human health risks. *Sci. Total Environ.* **2018**, *621*, 1093–1102. [[CrossRef](#)]
30. Asimakopoulos, A.G.; Wang, L.; Thomaidis, N.S.; Kannan, K. Benzotriazoles and benzothiazoles in human urine from several countries: A perspective on occurrence, biotransformation, and human exposure. *Environ. Int.* **2013**, *59*, 274–281. [[CrossRef](#)]
31. Pillard, D.A.; Cornell, J.S.; DuFresne, D.L.; Hernandez, M.T. Toxicity of Benzotriazole and Benzotriazole Derivatives to Three Aquatic Species. *Water Res.* **2001**, *35*, 557–560. [[CrossRef](#)]
32. Samuel, J.J. Photocatalytic degradation of methylene blue under visible light by dye sensitized titania Photocatalytic degradation of methylene blue under visible light by dye sensitized titania. *Mater. Res. Express* **2020**, *7*, 015051. [[CrossRef](#)]
33. Islam, M.T.; Dominguez, A.; Turley, R.S.; Kim, H.; Sultana, K.A.; Shuvo, M.A.I.; Alvarado-Tenorio, B.; Montes, M.O.; Lin, Y.; Gardea-Torresdey, J.; et al. Development of photocatalytic paint based on TiO<sub>2</sub> and photopolymer resin for the degradation of organic pollutants in water. *Sci. Total Environ.* **2020**, *704*, 135406. [[CrossRef](#)] [[PubMed](#)]
34. Tschirch, J.; Dillert, R.; Bahnemann, D.; Proft, B.; Biedermann, A.; Goer, B. Photodegradation of methylene blue in water, a standard method to determine the activity of photocatalytic coatings? *Res. Chem. Intermed.* **2008**, *34*, 381–392. [[CrossRef](#)]
35. Gao, B.; Chen, G.Z.; Puma, G.L. Carbon nanotubes/titanium dioxide (CNTs/TiO<sub>2</sub>) nanocomposites prepared by conventional and novel surfactant wrapping sol-gel methods exhibiting enhanced photocatalytic activity. *Appl. Catal. B Environ.* **2009**, *89*, 503–509. [[CrossRef](#)]
36. Kwon, C.H.; Shin, H.; Kim, J.H.; Choi, W.S.; Yoon, K.H. Degradation of methylene blue via photocatalysis of titanium dioxide. *Mater. Chem. Phys.* **2004**, *86*, 78–82. [[CrossRef](#)]
37. Ono, Y.; Rachi, T.; Okuda, T.; Yokouchi, M.; Kamimoto, Y.; Nakajima, A.; Okada, K. Kinetics study for photodegradation of methylene blue dye by titanium dioxide powder prepared by selective leaching method. *J. Phys. Chem. Solids* **2012**, *73*, 343–349. [[CrossRef](#)]
38. Ertuğ, E.B.; Vakifahmetoglu, C.; Öztürk, A. Enhanced methylene blue removal efficiency of TiO<sub>2</sub> embedded porous glass. *J. Eur. Ceram. Soc.* **2020**, *41*, 1530–1536. [[CrossRef](#)]
39. Shidpour, R.; Simchi, A.; Ghanbari, F.; Vossoughi, M. Photo-degradation of organic dye by zinc oxide nanosystems with special defect structure: Effect of the morphology and annealing temperature. *Appl. Catal. A Gen.* **2014**, *472*, 198–204. [[CrossRef](#)]
40. Yang, C.; Dong, W.; Cui, G.; Zhao, Y.; Shi, X.; Xia, X.; Tang, B.; Wang, W. Highly efficient photocatalytic degradation of methylene blue by P2ABSA-modified TiO<sub>2</sub> nanocomposite due to the photosensitization synergetic effect of TiO<sub>2</sub> and P2ABSA. *RSC Adv.* **2017**, *7*, 23699–23708. [[CrossRef](#)]
41. National Center for Biotechnology Information PubChem Compound Summary for CID 6099, Methylene blue. Available online: <https://pubchem.ncbi.nlm.nih.gov/compound/Methylene-blue#section=Use-and-Manufacturing> (accessed on 15 November 2020).
42. Anwar, D.I.; Mulyadi, D. Synthesis of Fe-TiO<sub>2</sub> Composite as a Photocatalyst for Degradation of Methylene Blue. *Procedia Chem.* **2015**, *17*, 49–54. [[CrossRef](#)]
43. Savić, T.D.; Carević, M.V.; Mitrić, M.N.; Kuljanin-Jakovljević, J.Ž.; Abazović, N.D.; Čomor, M.I. Simulated solar light driven performance of nanosized ZnIn<sub>2</sub>S<sub>4</sub>/dye system: Decolourization vs. photodegradation. *J. Photochem. Photobiol. A Chem.* **2020**, *388*, 112154. [[CrossRef](#)]
44. Zhang, T.; Oyama, T.; Aoshima, A.; Hidaka, H.; Zhao, J.; Serpone, N. Photooxidative N-demethylation of methylene blue in aqueous TiO<sub>2</sub> dispersions under UV irradiation. *J. Photochem. Photobiol. A Chem.* **2001**, *140*, 163–172. [[CrossRef](#)]
45. Mahmoud, W.M.M.; Rastogi, T.; Kümmerer, K. Application of titanium dioxide nanoparticles as a photocatalyst for the removal of micropollutants such as pharmaceuticals from water. *Curr. Opin. Green Sustain. Chem.* **2017**, *6*, 1–10. [[CrossRef](#)]

46. Khan, M.M.; Pradhan, D.; Sohn, Y. Springer Series on Polymer and Composite Materials Nanocomposites for Visible Light-induced Photocatalysis. In *Nanocomposites Visible Light. Photocatal*; Springer: Cham, Switzerland, 2017; pp. 19–40. [[CrossRef](#)]
47. Grčić, I.; Marčec, J.; Radetić, L.; Radovan, A.-M.; Melnjak, I.; Jajčinović, I.; Brnardić, I. Ammonia and methane oxidation on TiO<sub>2</sub> supported on glass fiber mesh under artificial solar irradiation. *Environ. Sci. Pollut. Res.* **2020**, *28*, 18354–18367. [[CrossRef](#)]
48. Racovita, A.D. Titanium Dioxide: Structure, Impact, and Toxicity. *Int. J. Environ. Res. Public Health* **2022**, *19*, 5681. [[CrossRef](#)]
49. Casado, C.; García-Gil, Á.; van Grieken, R.; Marugán, J. Critical role of the light spectrum on the simulation of solar photocatalytic reactors. *Appl. Catal. B Environ.* **2019**, *252*, 1–9. [[CrossRef](#)]
50. Khalid, N.R.; Majid, A.; Tahir, M.B.; Niaz, N.A.; Khalid, S. Carbonaceous-TiO<sub>2</sub> nanomaterials for photocatalytic degradation of pollutants: A review. *Ceram. Int.* **2017**, *43*, 14552–14571. [[CrossRef](#)]
51. Woan, K.; Pyrgiotakis, G.; Sigmund, W. Photocatalytic carbon-nanotube-TiO<sub>2</sub> composites. *Adv. Mater.* **2009**, *21*, 2233–2239. [[CrossRef](#)]
52. Malinowski, S.; Presečki, I.; Jajčinović, I.; Brnardić, I.; Mandić, V.; Grčić, I. Intensification of Dihydroxybenzenes Degradation over Immobilized TiO<sub>2</sub> Based Photocatalysts under Simulated Solar Light. *Appl. Sci.* **2020**, *10*, 7571. [[CrossRef](#)]
53. Marques, R.R.N.; Sampaio, M.J.; Carrapiço, P.M.; Silva, C.G.; Morales-Torres, S.; Dražić, G.; Faria, J.L.; Silva, A.M.T. Photocatalytic degradation of caffeine: Developing solutions for emerging pollutants. *Catal. Today* **2013**, *209*, 108–115. [[CrossRef](#)]
54. Sundar, K.P.; Kanmani, S. Progression of Photocatalytic reactors and it's comparison: A Review. *Chem. Eng. Res. Des.* **2020**, *154*, 135–150. [[CrossRef](#)]
55. Zhao, D.; Yang, X.; Chen, C.; Wang, X. Enhanced photocatalytic degradation of methylene blue on multiwalled carbon nanotubes-TiO<sub>2</sub>. *J. Colloid Interface Sci.* **2013**, *398*, 234–239. [[CrossRef](#)] [[PubMed](#)]
56. Pava-Gómez, B.; Vargas-Ramírez, X.; Díaz-Urbe, C.; Romero, H.; Duran, F. Evaluation of copper-doped TiO<sub>2</sub> film supported on glass and LDPE with the design of a pilot-scale solar photoreactor. *Sol. Energy* **2021**, *220*, 695–705. [[CrossRef](#)]
57. Mani, S.S.; Rajendran, S.; Nalajala, N.; Mathew, T.; Gopinath, C.S. Electronically Integrated Mesoporous Ag-TiO<sub>2</sub> Nanocomposite Thin films for Efficient Solar Hydrogen Production in Direct Sunlight. *Energy Technol.* **2022**, *10*, 2100356. [[CrossRef](#)]
58. Rodríguez-Acosta, J.W.; Mueses, M.Á.; Machuca-Martínez, F. Mixing Rules Formulation for a Kinetic Model of the Langmuir-Hinshelwood Semipredictive Type Applied to the Heterogeneous Photocatalytic Degradation of Multicomponent Mixtures. *Int. J. Photoenergy* **2014**, *2014*, 817538. [[CrossRef](#)]
59. Muñoz-Flores, P.; Poon, P.S.; Ania, C.O.; Matos, J. Performance of a C-containing Cu-based photocatalyst for the degradation of tartrazine: Comparison of performance in a slurry and CPC photoreactor under artificial and natural solar light. *J. Colloid Interface Sci.* **2022**, *623*, 646–659. [[CrossRef](#)] [[PubMed](#)]
60. Marić, T. Aging of Photocatalysis Based on Titanium (IV) Oxide and Carbon Nanotubes. Master's Thesis, University of Zagreb, Zagreb, Croatia, 2020.
61. Anisuzzaman, S.M.; Joseph, C.G.; Pang, C.K.; Affandi, N.A.; Maruja, S.N.; Vijayan, V. Current Trends in the Utilization of Photolysis and Photocatalysis Treatment Processes for the Remediation of Dye Wastewater: A Short Review. *ChemEngineering* **2022**, *6*, 58. [[CrossRef](#)]
62. Vaya, D.; Surolija, P.K. Semiconductor based photocatalytic degradation of pesticides: An overview. *Environ. Technol. Innov.* **2020**, *20*, 101128. [[CrossRef](#)]
63. Kurwadkar, S.; Evans, A.; DeWinne, D.; White, P.; Mitchell, F. Modeling photodegradation kinetics of three systemic neonicotinoids-dinotefuran, imidacloprid, and thiamethoxam-in aqueous and soil environment. *Environ. Toxicol. Chem.* **2016**, *35*, 1718–1726. [[CrossRef](#)]
64. Herrmann, J.-M. Photocatalysis. In *Kirk-Othmer Encyclopedia of Chemical Technology*; John Wiley & Sons, Inc.: Hoboken, NJ, USA, 2017; pp. 1–44, ISBN 9780128105252.
65. Pérez-Estrada, L.A.; Maldonado, M.I.; Gernjak, W.; Agüera, A.; Fernández-Alba, A.R.; Ballesteros, M.M.; Malato, S. Decomposition of diclofenac by solar driven photocatalysis at pilot plant scale. *Catal. Today* **2005**, *101*, 219–226. [[CrossRef](#)]
66. Shorgoli, A.A.; Shokri, M. Photocatalytic degradation of imidacloprid pesticide in aqueous solution by TiO<sub>2</sub> nanoparticles immobilized on the glass plate. *Chem. Eng. Commun.* **2017**, *204*, 1061–1069. [[CrossRef](#)]
67. Liang, R.; Tang, F.; Wang, J.; Yue, Y. Photo-degradation dynamics of five neonicotinoids: Bamboo vinegar as a synergistic agent for improved functional duration. *PLoS ONE* **2019**, *14*, e0223708. [[CrossRef](#)] [[PubMed](#)]
68. Ye, J.; Zhou, P.; Chen, Y.; Ou, H.; Liu, J.; Li, C.; Li, Q. Degradation of 1H-benzotriazole using ultraviolet activating persulfate: Mechanisms, products and toxicological analysis. *Chem. Eng. J.* **2018**, *334*, 1493–1501. [[CrossRef](#)]
69. Liu, X.; Wang, X.; Xing, X.; Li, Q.; Yang, J. Visible light photocatalytic activities of carbon nanotube/titanic acid nanotubes derived-TiO<sub>2</sub> composites for the degradation of methylene blue. *Adv. Powder Technol.* **2015**, *26*, 8–13. [[CrossRef](#)]
70. Elghniji, K.; Ksibi, M.; Elaloui, E. Sol-gel reverse micelle preparation and characterization of N-doped TiO<sub>2</sub>: Efficient photocatalytic degradation of methylene blue in water under visible light. *J. Ind. Eng. Chem.* **2012**, *18*, 178–182. [[CrossRef](#)]
71. de la Flor, M.P.; Camarillo, R.; Martínez, F.; Jiménez, C.; Quiles, R.; Rincón, J. Synthesis and characterization of TiO<sub>2</sub>/CNT/Pd: An effective sunlight photocatalyst for neonicotinoids degradation. *J. Environ. Chem. Eng.* **2021**, *9*, 106278. [[CrossRef](#)]
72. Speltini, A.; Maraschi, F.; Sturini, M.; Contini, M.; Profumo, A. Dispersive multi-walled carbon nanotubes extraction of benzenesulfonamides, benzotriazoles, and benzothiazoles from environmental waters followed by microwave desorption and HPLC-HESI-MS/MS. *Anal. Bioanal. Chem.* **2017**, *409*, 6709–6718. [[CrossRef](#)]

73. Martínez, C.; Canle, L.M.; Fernández, M.I.; Santaballa, J.A.; Faria, J. Kinetics and mechanism of aqueous degradation of carbamazepine by heterogeneous photocatalysis using nanocrystalline TiO<sub>2</sub>, ZnO and multi-walled carbon nanotubes–anatase composites. *Appl. Catal. B Environ.* **2011**, *102*, 563–571. [[CrossRef](#)]
74. Cao, Q.; Yu, Q.; Connell, D.W.; Yu, G. Titania/carbon nanotube composite (TiO<sub>2</sub>/CNT) and its application for removal of organic pollutants. *Clean Technol. Environ. Policy* **2013**, *15*, 871–880. [[CrossRef](#)]
75. Yao, Y.; Luan, J. Preparation, Property Characterization of Gd<sub>2</sub>YSbO<sub>7</sub>/ZnBiNbO<sub>5</sub> Heterojunction Photocatalyst for Photocatalytic Degradation of Benzotriazole under Visible Light Irradiation. *Catalysts* **2022**, *12*, 159. [[CrossRef](#)]
76. Čižmar, T.; Panžić, I.; Capan, I.; Gajović, A. Nanostructured TiO<sub>2</sub> photocatalyst modified with Cu for improved imidacloprid degradation. *Appl. Surf. Sci.* **2021**, *569*, 151026. [[CrossRef](#)]
77. Bohač, M.; Čižmar, T.; Kojić, V.; Marčec, J.; Juraić, K.; Grčić, I.; Gajović, A. Novel, Simple and Low-Cost Preparation of Ba-Modified TiO<sub>2</sub> Nanotubes for Diclofenac Degradation under UV/Vis Radiation. *Nanomaterials* **2021**, *11*, 2714. [[CrossRef](#)] [[PubMed](#)]
78. Chen, Y.; Ye, J.; Li, C.; Zhou, P.; Liu, J.; Ou, H. Degradation of 1 H -benzotriazole by UV/H<sub>2</sub>O<sub>2</sub> and UV/TiO<sub>2</sub>: Kinetics, mechanisms, products and toxicology. *Environ. Sci. Water Res. Technol.* **2018**, *4*, 1282–1294. [[CrossRef](#)]
79. Nekouei, S.; Nekouei, F. Comparative procedure of photodegradation of methylene blue using N doped activated carbon loaded with hollow 3D flower like ZnS in two synergic phases of adsorption and catalytic. *J. Photochem. Photobiol. A Chem.* **2018**, *364*, 262–273. [[CrossRef](#)]
80. Salavati, H.; Kohestani, T. Preparation, characterization and photochemical degradation of dyes under UV light irradiation by inorganic–organic nanocomposite. *Mater. Sci. Semicond. Process.* **2013**, *16*, 1904–1911. [[CrossRef](#)]
81. Ji, K.H.; Jang, D.M.; Cho, Y.J.; Myung, Y.; Kim, H.S.; Kim, Y.; Park, J. Comparative Photocatalytic Ability of Nanocrystal-Carbon Nanotube and -TiO<sub>2</sub> Nanocrystal Hybrid Nanostructures. *J. Phys. Chem. C* **2009**, *113*, 19966–19972. [[CrossRef](#)]
82. Grčić, I.; Papić, S.; Brnardić, I. Photocatalytic Activity of TiO<sub>2</sub> Thin Films: Kinetic and Efficiency Study. *Int. J. Chem. React. Eng.* **2018**, *16*, 20160153. [[CrossRef](#)]